Active Vertical Stabilization Mechanism for Lightweight Handheld Cameras

Ali Utku Pehlivan
Disney Research Los Angeles
aupehlivan@gmail.com

Günter Niemeyer
Disney Research Los Angeles
gunter.niemeyer@disneyresearch.com

Abstract

Camera technology is continuously improving and high quality cameras are now available under one pound of weight. This enables novel and innovative uses, for example at the end of a long boom pole. Unfortunately lighter cameras used in such ways are more susceptible to vertical disturbances and the bouncing associated with walking resulting in shaking and distortion. We introduce a miniaturized active stabilization mechanism that attenuates such disturbances and keeps the camera steady. Feedback control effectively emulates the stabilizing inertial dynamics associated with higher weights without the penalty of higher weight. The system uses only accelerometer readings and avoids pure integration and associated numerical drift issues. We design, analyze, build, and test the mechanism to show appropriate performance.

Figure 1: A lightweight camera on a 3dof active gimbal and boom is susceptible to vertical disturbances.

1. Introduction

Camera operators are always trying to capture new and unique camera perspectives. To facilitate their efforts, we recently placed a small form factor camera at the end of an eight foot hand-held boom pole [1]. The system, seen in Fig. 1, includes an active three degree of freedom (3 dof) gimbal to stabilize the camera orientation. Unfortunately, the camera remains susceptible to vertical translation disturbances, caused mostly by walking and exasperated by the boom length. It is our objective to stabilize against such disturbances.

Mechanical stabilization systems for portable cameras have been commercially available since the 1970s. Large camera inertias and even added weights mechanically filter out any disturbances. A widely known example, Steadicam, transfers the heavy weight directly to the operator's body [2, 3]. The mechanism utilizes strategically placed springs for the gravity compensation over a large range of motion and adds a camera gimbal beyond the stabilization.

In our application, the boom's flexibility and free movement require the stabilization mechanism to be miniaturized and located at the tip of the boom. A purely passive approach is not applicable for two main reasons. First, the camera weight has to be at least an order of magnitude smaller, substantially reducing the efficacy of passive inertial stabilization. Second, the mechanism's range of motion is much smaller than the possible vertical movements. So the system needs to include some restoring stiffness to keep the camera in the travel range. A purely passive stiffness, together with the low mass, would raises the passive filtering's cutoff frequency and again decreases efficacy. Finally, attached to a moving boom, a vertical reference is not naturally available.

In this work, we develop an active miniaturized stabilization mechanism, aimed to be integrated within an active gimbal. Effectively, the system creates the dynamics of a large camera inertia without the penalty of weight needed to be carried. We are able to avoid pure integration of the accelerometer signal and any as-

sociated numerical drift, achieving height stabilization without a direct height measurement.

The paper first states the design specifications in terms of desired attenuation of vertical disturbances. It then presents the mechanical structure of a possible extended gimbal and analyzes the required passive gravity compensation elements. It also derives the active controller and accelerometer usage. A final experimental evaluation is followed by a brief discussion and concluding remarks.

2. Design Specifications

The developed mechanism acts as a low pass filter, isolating the camera from unintended movements in the vertical direction. To specify the necessary attenuation, we examine both the expected disturbances as well as the necessary smoothness.

To characterize possible disturbances, we observed two unexperienced operators holding a fully extended boom and walking at a comfortable speed. Both operators held the boom in three different orientations (vertically, horizontally, and at approximately 45°), walked forwards, backwards, and sideways, and repeated each scenario three times for 27 tests each. An OptiTrack optical motion capture system recorded the boom tip's motion, with example trajectories shown in Fig. 2(b).

Based on a power spectral density analysis of the tip motion, we see the largest power in the range 0.5-1.0Hz (Fig. 2(a)). To find the matching signal amplitude, we integrated the total power in this frequency range corresponding to the signal variance, σ^2. And given a fairly periodic disturbance, we estimate the average signal's amplitude as 2σ. This compromises between the smaller $\sqrt{2}\sigma$ amplitude a pure sinusoid would exhibit and the 3σ amplitude a totally random signal might generate [4]. The resulting disturbance amplitudes across holding cases and subjects are presented in Table 1. Overall, we expect the vertical disturbances to show amplitudes up to 0.032m within the frequency range of 0.5-1Hz.

To define the desired stabilization smoothness, we visually compared photos taken from different heights. In particular, as the camera moves vertically the foreground shifts relative to the background. The just noticeable difference places a bound on acceptable height variations. In our tests, sampled in Fig. 3, we placed a lamp as foreground 2m from the camera. A 1mm displacement was not noticeable, while a 5mm displacement was clearly noticeable. As the perspective change can be approximated by translating the foreground, it is not surprising that a 1mm shift at a 2m distance is unnoticeable.

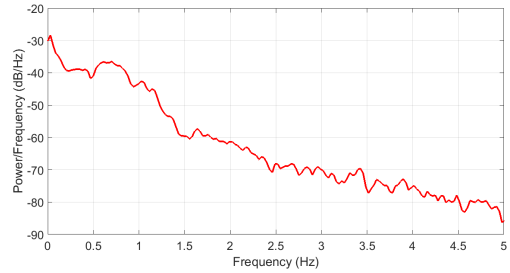

(a)

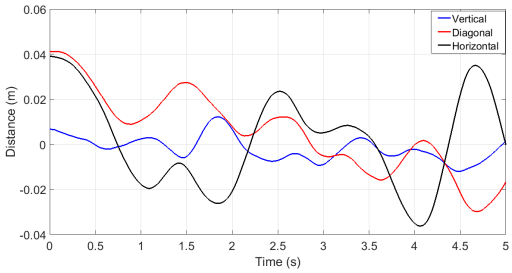

(b)

Figure 2: Characterization of expected disturbances (a) Power spectral density and (b) Sample trajectories of the boom tip vertical movements.

Table 1: Disturbance amplitudes across subjects and holding cases.

Subject	Vertical	Diagonal	Horizontal
S1	0.027m	0.026m	0.032m
S2	0.013m	0.024m	0.022m

Consequently, we desire the stabilization mechanism to attenuate the vertical disturbances by a factor 10 or more, from 0.013-0.032m to under 3mm (ideally 1mm) within the 0.5-1Hz frequency range.

3. Integrated Gimbal Structure

The miniaturized active stabilization mechanism is intended to be used within a gimbal structure. Here we review a proposed integrated gimbal to gain insight into the development of the stabilization mechanism.

The integrated active gimbal combines the active miniaturized stabilization with roll-pitch joints and a pan-tilt platform into a 5 dof mechanism (Fig. 4). All degrees of freedom are necessary to provide a vertical reference to the stabilization. Assume the boom may be rolled and held at any angle. Numbered outward from the boom to the camera, the axes 1 and 2 provide roll and pitch joints such that axis 3 is always vertical. Axis

(a) (b) (c)

Figure 3: Sample camera images showing: (a) the base image, (b) a 1mm shift, (c) a 5mm shift. For illustrative purposes, the shifted images are darkened and overlaid with computed differences in yellow. The actual comparisons were performed alternately viewing images in the same location, simulating a video stream.

3 and 5 together then function as pan and tilt to orient the camera while keeping it level. And axis 4, using a leverarm to the camera, imparts and stabilizes vertical movements.

While theoretically redundant to control camera orientation and vertical displacement, the kinematic structure isolated in Fig. 4(a) offers several key benefits. First, once the camera's center of mass is perfectly aligned with the axes 3 and 5, hence only axis 4 sees any gravitational loads. Second, as axis 3 provides a vertical reference, the gravity load on axis 4 can be offset by a passive compensation as described below. Together this relaxes the strength needs, size, and ultimately weight of all actuators.

Furthermore, sandwiching the stabilization inside the pan-tilt platform allows the tilt axis 5 to actively counter tilt variations imparted by the axis 4. We can avoid the typical parallelogram arrangements employed to isolate vertical stabilization from orientation. This again reduces size, weight, number of moving parts, and thus friction of the design.

Finally, the redundancy helps avoid singular positions or gimbal lock during normal operations. The boom and camera can independently point in any direction, with the possible exception of exact vertical orientations.

Dynamically, to ensure smooth motions we aim to decrease friction on all axes as much as possible by employing brushless direct drive actuators. Without gravity loading, the expected torques are quite small and we target actuators with a 0.1Nm continuous torque limit.

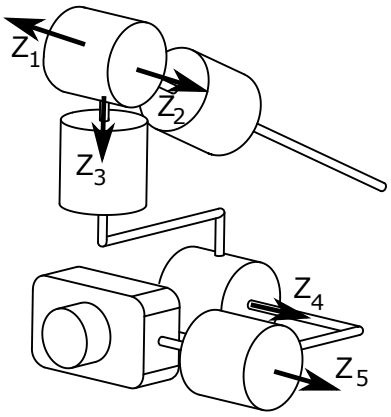

(a)

(b)

Figure 4: The proposed integrated active gimbal: (a) the kinematic structure, and (b) a computer aided design (CAD) model. Note the CAD model does not yet include a 5th axis.

In this study we focus on the active vertical stabilization mechanism built around axis 4. We remember, however, that the design is intended to fit inside the integrated active gimbal.

4. Gravity Compensation Mechanism

To support the overall stabilization and reduce the required actuator torques, we implement a passive gravity compensation mechanism. This mechanism should balance as much of the load's weight as possible while introducing as little friction and added complexity as necessary. The final tilt actuator rotates the camera about its center of mass, so for the purpose of this mechanism design we can consider the load to be a point mass m on a lever arm moving $\pm 45^\circ$ about a horizontal nominal orientation. In the following derivation, all angles are measured clockwise relative to this horizontal orientation.

Perfect gravitational compensation can be realized using a counter-balance mass with no added friction and very little complexity [5]. Unfortunately the added weight is prohibitive in this application and we focus on spring-based designs. Perfect spring compensation requires anchoring an ideal spring above the leverarm's pivot point, as shown in Fig. 5. To confirm the result, consider the potential energies of gravity

$$E_{\text{grav}} = -mg\, r\sin(\theta) \tag{1}$$

and the spring

$$E_{\text{spring}} = \tfrac{1}{2}kL^2 = \tfrac{1}{2}k\left(d^2 + r^2 - 2dr\cos(\theta + 90^\circ)\right) \tag{2}$$

The changes in energy exactly balance if

$$d = \frac{mg}{k} \tag{3}$$

which can easily be fine-tuned with a slightly variable anchor point.

Unfortunately exact compensation requires an ideal zero free-length spring for which the stored energy and torque reach zero at exactly zero length. Such springs are extremely hard to manufacture and not practical. Thus many gravity compensation designs use cable and pulley systems or linkages to hide the spring's rest length and mimic the above layout [6]. These generally add friction, complexity, and weight. We therefore target approximate compensation designs, shifting the spring anchor point and possibly combining two springs. Without moving parts, we can minimize friction and weight while optimizing the compensation.

Consider conventional springs with a rest or free length L_0. Anchor the springs a distance d from the pivot point and an angle β from horizontal, as shown in Fig. 6. First evaluate a single spring, depicted in red. From trigonometry, the spring length is

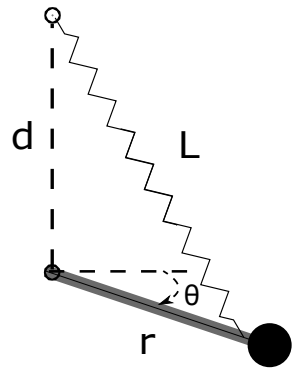

Figure 5: Idealized passive gravity compensation.

$$L = \sqrt{d^2 + r^2 - 2dr\cos(\theta - \beta)} \tag{4}$$

where we recall angles to be measured clockwise from horizontal. The effective leverarm or distance to the pivot point is

$$\begin{aligned} h &= \frac{1}{L}\sqrt{d^2r^2 - \tfrac{1}{4}\left(d^2 + r^2 - L^2\right)^2} \\ &= \frac{d\ r\ \sin(\theta - \beta)}{L} \end{aligned} \tag{5}$$

so that the compensation torque is

$$\tau(d,\beta) = k\,\frac{L - L_0}{L}\,dr\,\sin(\theta - \beta) \tag{6}$$

Using the parameters of the physical system (r=0.075m, m=0.895kg, k=120N/m, L_0=0.05m) we achieve the minimal maximum error to balance gravity across the $\pm 45^\circ$ workspace for d=0.116m and β=-101°. The resultant compensation is graphed in Fig. 7(a) with a maximum error of 0.077Nm or 11.7% of the maximum gravity torque. For reference, the actuators can deliver 0.1Nm allowing the active controller to account for the residual errors.

Notice that the spring takes a length of 0.149m at the nominal position. This leads to a design somewhat larger than desired as it expands the size of the surrounding gimbal. A stiffer spring could create a more compact layout, at the expense of increased sensitivity and likely larger errors in practice. To further improve the compensation we consider the use of a second, corrective spring.

Optimizing a dual-spring configuration for minimal maximum error, we see two even larger springs

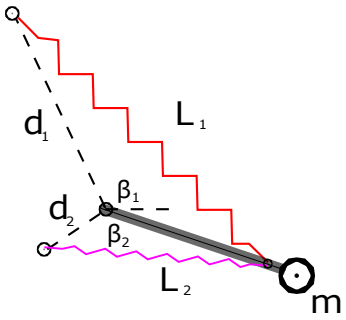

Figure 6: Approximate Spring-Based Gravity Compensation.

	Anchor Point		Nominal Spring	Maximum
	Distance	Angle	Length	Error
Single Spring	0.116m	-101°	0.149m	0.077Nm
Dual Spring	0.155m	-95°	0.172m	0.0017Nm
Error-Optimized	0.070m	112°	0.150m	
Dual Spring	0.100m	-90°	0.125m	0.084Nm
Size-Optimized	0.055m	154°	0.127m	

Table 2: Gravity Compensation Design Parameters. The spring's anchor point as well as length at the nominal lever location convey a sense of the design's size. The maximum torque error describes the compensation quality.

counteracting each other. The parameters are collected in Table 2. The resultant compensation is improved with a maximum error of 0.0017Nm, as seen in Fig. 7(b). In practice however, the larger size increases overall dimensions and weight.

A more compact design is achieved when restricting $\beta_1 = -90^\circ$, that is attaching the primary spring above the pivot point. The first (primary) spring leaves a large error which the second spring is able to correct. The resultant design is smaller than the single-spring solution, while achieving an equally good compensation, shown in Fig. 7(c). This was implemented and used in the demonstration system.

5. Active Vertical Stabilization

In theory, if the camera were perfectly suspended, its inertia would keep it stationary regardless of the base or boom movements. However, given all imperfections and the relatively low inertia, we need to implement an active stabilization to reinforce the natural dynamics. As such, the following controller creates an artificially large inertia and rejects forces due to imperfections in the gravity compensation, friction, wiring and other disturbances. In addition, as the boom can move vertically over several meters, the camera must gradually re-equilibrate and follow the boom's low-speed vertical movements.

Sensing of the vertical movements with respect to ground is challenging at best. Lidar, ultrasound, or pressure sensors can be confused by their surroundings and give false readings. Accelerometers are insensitive to the environment but obtaining position via double integration involves significant challenges [7], such as extreme sensitivity to DC offset, which leads up to measurement drift. Fortunately, the following scheme enables accelerometer feedback without pure integration.

Consider the vertical stabilization joint shown in Fig. 8 with

$$\Delta x = x_{\text{base}} - x_{\text{cam}} \tag{7}$$

If we desire the dynamics of a large inertia m_d as well as a low re-equilibrating stiffness K_d and damping B_d

$$m_d \ddot{x}_{\text{cam}} = B_d(\dot{x}_{\text{base}} - \dot{x}_{\text{cam}}) + K_d(x_{\text{base}} - x_{\text{cam}}) \tag{8}$$

we should assert the filtering transfer function

$$\frac{X_{\text{cam}}}{X_{\text{base}}} = \frac{B_d s + K_d}{m_d s^2 + B_d s + K_d} = \frac{2\xi\omega_n s + \omega_n^2}{s^2 + 2\xi\omega_n s + \omega_n^2} \tag{9}$$

Greater stabilization with a larger desired inertia and a softer virtual spring implies a lower cutoff frequency. The corresponding deflection Δx would obey

$$\Delta X = \frac{s^2\, X_{\text{base}}}{s^2 + 2\xi\omega_n s + \omega_n^2} = \frac{s^2\, X_{\text{cam}}}{2\xi\omega_n s + \omega_n^2} \tag{10}$$

We see the desired dynamics (8) relate the deflection directly to acceleration. We place an accelerometer on the base side of the actuator to leverage the greater filtering and inherently provide a control signal from the observed disturbance. From $a = \ddot{x}_{\text{base}}$ we compute a desired deflection

$$\frac{\Delta X_d}{A} = H(s) = \frac{1}{s^2 + 2\xi\omega_n s + \omega_n^2} \tag{11}$$

and a desired joint angle

$$\theta_d = \sin^{-1}\frac{\Delta x_d}{r} \approx \frac{\Delta x_d}{r} \tag{12}$$

Using a proportional+derivative joint controller, the actual camera dynamics are governed by

$$m\ddot{x}_{\text{cam}} = b(\Delta\dot{x} - \Delta\dot{x}_d) + k(\Delta x - \Delta x_d) + F_{\text{dist}} \tag{13}$$

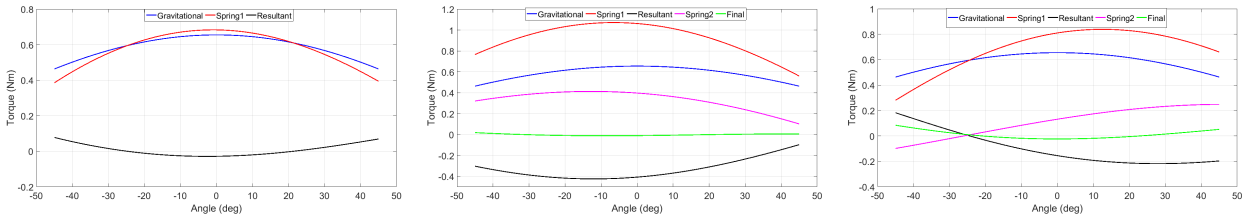

(a) Single Spring (b) Dual Spring Error-Optimized (c) Dual Spring Size-Optimized

Figure 7: Gravity Compensation Torques over the workspace.

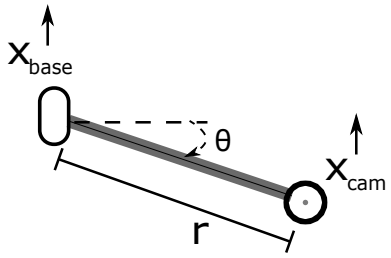

Figure 8: Vertical Stabilization Joint (with the gravity compensation mechanism not shown).

where the actual mass m is subject to the effective controller gains b and k as well as force disturbances F_{dist}. Substituting (11) we find the closed-loop dynamics

$$\begin{aligned} X_{\text{cam}} &= \frac{bs+k}{ms^2+bs+k}\,\frac{2\xi\,\omega_n s+\omega_n^2}{s^2+2\xi\,\omega_n s+\omega_n^2}\,X_{\text{base}} \\ &+ \frac{1}{ms^2+bs+k}\,F_{\text{dist}} \end{aligned} \tag{14}$$

High controller gains reject any disturbances while the low virtual stiff and high desired mass independently set ω_n to filter the unintended vertical movements.

6. Accelerometer Noise/Brownian Motion

The controller's filtering structure (11) avoids pure integration of the accelerometer and provides tolerance to sensor offsets. Unfortunately accelerometers also contain random sensor noise which, whether integrated or filtered, results in Brownian movements of the camera. In essence, the accelerometer signal-to-noise ratio determines how well small base movements can be rejected versus how much Brownian motion is injected.

Assume the accelerometer noise has a power spectral density $S_a(\omega)$ versus frequency $\omega = 2\pi f$. The variance of the accelerometer signal, being the square of the standard deviation σ_a and the expected value of $a(t)^2$, can be reconstructed from

$$\sigma_a^2 = E[a(t)^2] = \frac{1}{2\pi}\int_{-\infty}^{\infty} S_a(\omega)\,\mathrm{d}\omega \tag{15}$$

Meanwhile, when passed through the linear time-invariant (LTI) system $H(j\omega)$ given in (11), the power spectral density is shaped by

$$S_{\Delta x}(\omega) = |H(j\omega)|^2 S_a(\omega) \tag{16}$$

We can thus predict the variance of the vertical deflection due to accelerometer noise as

$$\sigma_{\Delta x}^2 = E[\Delta x(t)^2] = \frac{1}{2\pi}\int_{-\infty}^{\infty} |H(j\omega)|^2 S_a(\omega)\,\mathrm{d}\omega \tag{17}$$

For white accelerometer noise with a constant S_a

$$\sigma_{\Delta x}^2 = \frac{S_a}{2\pi}\int_{-\infty}^{\infty} \frac{1}{(\omega_n^2-\omega^2)^2+(2\xi\,\omega_n\omega)^2}\,\mathrm{d}\omega \tag{18}$$

and substituting $\nu = \omega/\omega_n$ we find

$$\begin{aligned} \sigma_{\Delta x}^2 &= \frac{S_a}{2\pi}\,\frac{1}{\omega_n^3}\int_{-\infty}^{\infty} \frac{1}{\nu^4+(4\xi^2-2)\nu^2+1}\,\mathrm{d}\nu \\ &= \frac{S_a}{2\pi}\,\frac{1}{\omega_n^3}\,\frac{\pi}{2\xi} = \frac{S_a}{4\xi\,\omega_n^3} \end{aligned} \tag{19}$$

The standard deviation of the joint deflection

$$\sigma_{\Delta x} = \frac{\sqrt{S_a}}{2\,\omega_n\,\sqrt{\xi\,\omega_n}} \tag{20}$$

is therefore both proportional to the standard deviation of the raw accelerometer signal as well as more than inversely proportional to the desired natural frequency. In Fig. 9 we take raw accelerometer readings while the system is at rest and compute the Brownian motion resulting from (11) for varying frequencies. This clearly shows the strong dependence on cutoff frequency.

7. Evaluation of the Mechanism

We evaluated the stabilization characteristics of the implemented system in a benchtop experiment. During

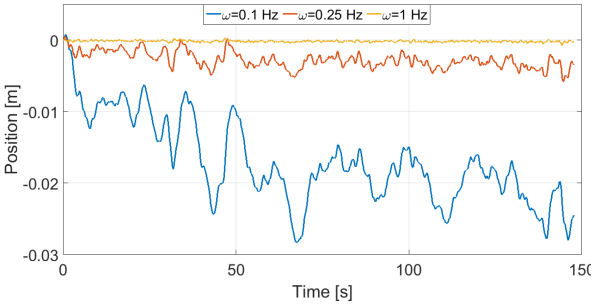

Figure 9: Brownian motion in the vertical deflection. Standard deviations are 5.9mm, 1.1mm and 0.12mm for the cutoff frequencies 0.1Hz, 0.25Hz abd 1 Hz, respectively.

the experiment the base of the stabilization mechanism moved on a linear slide, driven by a brushed DC actuator. The setup is shown in Fig. 11. The linear slide was excited with a 0.03 m peak to peak swept-sine wave with the frequency changing from 0.01 Hz to 3 Hz in 60 seconds. The motion of both the base and the camera were sensed via an OptiTrack optical motion capture system at a frequency of 120 Hz. The magnitude response of the system was created using the *tfestimate* function in MATLAB, and is plotted in Fig. 11. The stabilization mechanism decreases in the magnitude by 3 to 30 fold in the 0.5-1 Hz range.

8. Discussion and Conclusion

We presented the development of an active miniaturized stabilization mechanism. Unlike mechanical stabilization for portable cameras, which use large camera inertias to attenuate disturbances, our system achieves stabilization within a smaller dimension and for cameras at least an order of magnitude lighter. It combines a passive gravity compensation, optimized within the available space, with an active controller. The controller rejects any imperfections in the gravity compensation, friction, or other forces while creating the dynamics of a low virtual stiffness and high desired mass to filter the unintended vertical movements. For sensing, we employed only an accelerometer, avoiding pure integration of its signal and any associated numerical drift.

Practically, the noise in the accelerometer forces the trade off in the selection of the cut off frequency. To reject more disturbances and keep the camera stationary, we wish to reduce the cutoff frequency. But this increases the random Brownian motion caused by accelerometer noise. To achieve the desired disturbance rejection we target filtering at or below 0.1Hz. This

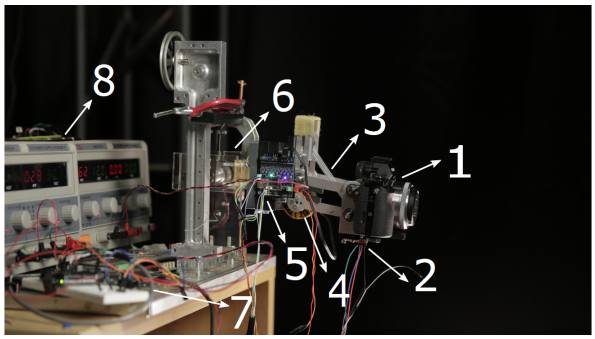

(a)

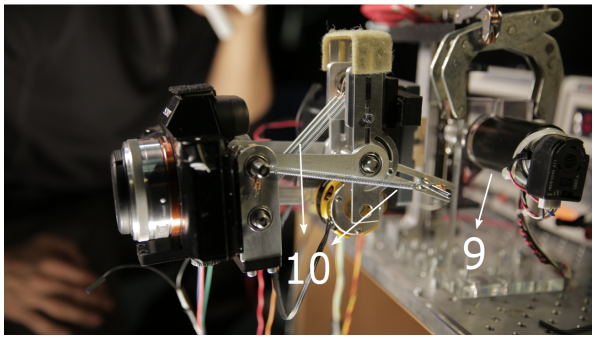

(b)

Figure 10: Experimental setup showing: (1) the camera, (2) a camera mounted accelerometer, (3) and (10) gravity compensation springs, (4) the brushless DC direct drive actuator, (5) the drive electronics and base accelerometer, (6) the vertical linear slide, (7) slide drive electronics, (8) power supply, and (9) slide drive actuator

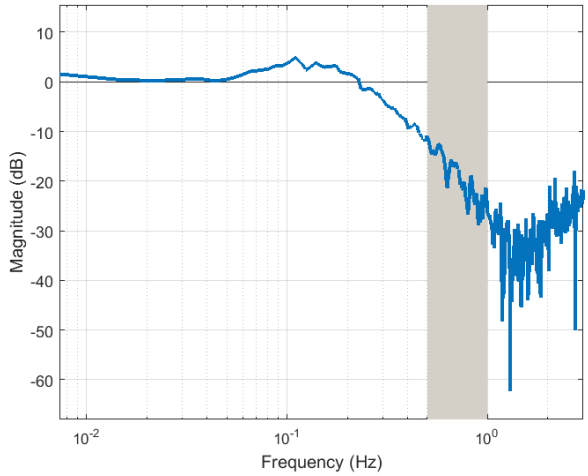

Figure 11: The experimental transfer function estimate shows a 3 to 30 fold attenuation in the 0.5-1 Hz range.

causes up to $\pm$10mm of Brownian motion with our accelerometer showing $400\mu g/\sqrt{\text{Hz}}$ noise. Fortunately, the latest generation accelerometers reduce noise nearly an order of magnitude to $50\mu g/\sqrt{\text{Hz}}$. We thus believe the newest sensors have reached the sweet spot necessary for practical operation.

We also note that the gravity compensation was optimized for our available spring stiffness k. From (3) we see stiffer springs could provide a more compact design. But such designs become more sensitive to tolerances and compensation errors grow more rapidly at the workspace extremes. Also, the design dimensions are more fundamentally dictated by the disturbance amplitudes. So we find the approximate design rules

$$r \geq (2-3)\text{disturbance amplitude} \tag{21}$$

$$k \approx \frac{mg}{r} \tag{22}$$

Finally, we presented the active controller with a linear virtual stiffness K_d. In practice fast vertical movements could drive the system past the available workspace. A nonlinear stiffening gain would help prevent impact into joint limits and create an appropriate amplitude-dependent filter cutoff.

Overall we are excited that camera and sensor technology has reached the threshold of enabling this miniaturized stabilization. We look forward to seeing these light weight and flexible systems slowly replace their heavy predecessors and disrupt the industry.

References

[1] V. Roberts and K. Salter, "Counterbalanced monopod jib for cameras," Patent, Aug. 9, 2016, U.S. Patent 9,411,214.

[2] G. W. Brown, "Equipment for use with hand held motion picture cameras," Patent, Apr. 12, 1977, U.S. Patent 4,017,168.

[3] S. Ferrara, *Steadicam: Techniques and aesthetics*. CRC Press, 2013.

[4] S. W. Smith *et al.*, *The scientist and engineer's guide to digital signal processing*. California Technical Pub. San Diego, 1997.

[5] J. P. Whitney and J. K. Hodgins, "A passively safe and gravity-counterbalanced anthropomorphic robot arm," in *2014 IEEE International Conference on Robotics and Automation (ICRA)*. IEEE, 2014, pp. 6168–6173.

[6] J. L. Herder, "Energy-free systems. theory, conception and design of statically balanced spring mechanisms," Ph.D. dissertation, Delft University of Technology, 2001.

[7] O. Celik, H. B. Gilbert, and M. K. O'Malley, "Dynamic displacement sensing, system identification, and control of a speaker-based tendon vibrator via accelerometers," *IEEE/ASME Transactions on Mechatronics*, vol. 18, no. 2, pp. 812–817, 2013.